N68-31042
(ACCESSION NUMBER) (THRU)

(PAGES) (CODE)

(NASA CR OR TMX OR AD NUMBER) (CATEGORY)

DEVELOPMENT OF A 1200-HERTZ ALTERNATOR AND CONTROLS FOR SPACE POWER SYSTEMS

by B. D. Ingle and C. S. Corcoran
Lewis Research Center
Cleveland, Ohio

JUL 1968
RECEIVED
NASA STI FACILITY
INPUT BRANCH

DEVELOPMENT OF A 1200-HERTZ ALTERNATOR

AND CONTROLS FOR SPACE POWER SYSTEMS

by B. D. Ingle and C. S. Corcoran

Lewis Research Center
Cleveland, Ohio

NATIONAL AERONAUTICS AND SPACE ADMINISTRATION

DEVELOPMENT OF A 1200-HERTZ ALTERNATOR AND CONTROLS FOR SPACE POWER SYSTEMS

by B. D. Ingle and C. S. Corcoran

Lewis Research Center
National Aeronautics and Space Administration
Cleveland, Ohio

ABSTRACT

For a 1200-hertz Brayton energy conversion system having a useful load rating of 10 kWe, an alternator and the associated voltage and frequency controls were designed and tested. The unique features in the components are:

(1) The 36,000-rpm solid-rotor alternator designed to accommodate gas bearings.

(2) Pulse-type voltage regulator which is synchronized with the line frequency.

(3) Multiple parasitic-loading speed control.

INTRODUCTION

The Lewis Research Center is currently developing a 10-kilowatt single-shaft Brayton energy conversion system. The working gas in this system is a mixture of helium and xenon with a molecular weight of approximately 83.8 and a pressure of approximately 40 pounds per square inch. One of the most critical assemblies in the system is the turbine-alternator-compressor which operates at 36,000 rpm on gas bearings. The purpose of this paper is to describe the development of the alternator and the electrical control packages in this system. In order to expedite component testing, a magnetic and thermal duplicate of the alternator but having ball bearings was constructed and tested. In addition to this test alternator, breadboard versions of the electrical controls were also built and tested, and the overall results of these tests are reported herein. Since this presentation is essentially an advance summary report, detailed component and electric system information will be reported in more detail at a later date.

Immediately preceding the development of this 1200-hertz single-shaft Brayton system, the electrical components for a two-shaft 400-hertz Brayton system were also investigated[1]. The 400-hertz system, which utilized an inductor alternator consisting of stationary coils and a solid rotor, was of the same general power level but was designed for operation at 12,000 rpm. The experience obtained with the 400-hertz Brayton system contributed significantly to the effectiveness of the 1200-hertz program. The high rotational speed and system pressure for the 1200-hertz Brayton system made desirable a smooth alternator rotor of a type characteristic of Lundell machines. This did not preclude the use of established design techniques.

Throughout the design phase of the program, component reliability was assigned the highest possibile priority, followed by the effort to maximize efficiency. Performance and weight were considered to be of less significance than either reliability or efficiency. It is of interest to note that the emphasis on reliability and efficiency makes it of prime importance to keep the alternator rotor small, for a small rotor decreases both the rotor stress and windage loss.

The development testing program consists of two phases. The first phase is component testing to determine such factors as efficiency, and off-design steady-state performance and temperature maps. The second phase consists of integrating the components into a subsystem to determine transient performance and component interactions.

The design, fabrication, and preliminary component testing of the alternator and the control packages were performed by the AiResearch Manufacturing Company, a division of the Carrett Corporation, under NASA Contract NAS3-9427.

It is recognized this report could not have been written without the contr butions of the below listed AiResearch engineering personnel. The contributions included the design and development of the alternator, shunt-field regulator, series-field controller, and the speed controllers.

AiResearch - Torrance, Calif.
F. B. McCarty
R. Rudich
AiResearch - Phoenix, Ariz.
K. P. Worcester
H. W. Longee

SYSTEM REQUIREMENTS

The major electrical components in the Brayton-cycle energy-conversion system, as shown in Fig. 1, consist of an alternator, a series-field controller, a shunt-field regulator and three parasitic-load speed controllers. Three speed controllers are utilized to improve system performance and to provide component redundancy.

The electrical rating of this Brayton Energy conver-

TM X-52453

sion system is 10 kilowatts, 120/208 volts, 3-phase 4-wire, 1200 hertz, and 0.8 power factor lagging in which the significant system characsitics include voltage regulation of ±1 percent, speed regulation of ±1 percent, maximum response times for voltage and speed of 1/4 and 1 second respectively, and maximum system efficiency over a 2.25 to 10.5 kW power range. A summary of the system performance goals (requirements) are listed in Table 1.

ALTERNATOR

The Brayton alternator is a solid-rotor modified-Lundell or Rice machine operating at 36,000 rpm, and designed to produce 10.7 kilowatts at 0.75 power factor with coolant inlet temperature at 70° F. The machine is hermetically sealed to prevent loss of the working gas in the system. Figure 2 is a sectional view of the alternator, showing: (1) the brazed bimetallic rotor, (2) the main gap, (3) the auxiliary gaps, (4) the armature, (5) the dual, stationary field coils, (6) the nonmagnetic armature separator, (7) the dual heat exchanger and (8) the heat shield.

It is interesting to note that this machine is a sophisticated version of the dynamo patented by Mr. Lewis B. Rice in 1897. The rotor of the alternator consists of two separate magnetic sections with two north poles on one section and two south poles on the other. To obtain a smooth, high-strength rotor, the interpolar space is a nonmagnetic metal. The flux path is shown by the arrows in figure 2. The flux enters the armature stack opposite the north poles, flows around the stack and re-enters the rotor at the south poles which are displaced by 90 degrees. The path is then completed through the auxiliary gaps, bells and frame. The armature winding thus sees an alternating flux as in a conventional salient pole machine. The function of the nonmagnetic separator around the stack is to minimize the leakage of flux into the frame. This flux leakage would occur for instance if the excitation circuits at each end were not balanced magnetically.

The advantages of this machine are the smooth rotor which minimizes the windage loss and the short armature coils when compared to the homopolar inductor alternator.

The following are a few of the unique design features incorporated in this machine: (1) Two fields, one for series excitation and the other for shunt excitation are utilized in the alternator. The series winding produces a magnetomotive force which is proportional to the alternator line current. The shunt winding produces the magnetomotive force as required to maintain the alternator output voltage at the desired level. The use of a series-field controller reduces, substantially, the requirements on the voltage regulator. Each field consists of two field coils as shown in Fig. 2. (2) The brazed, dual helix, heat exchanger provides redundant cooling paths in the event of failure of the primary cooling system, either internal or external to the alternator. (3) The brazed smooth-rotor construction provides a low windage loss

surface with sharp magnetic to nonmagnetic interfaces. (4) Each armature coil side in the slots is completely wrapped with insulation to minimize the current leakage around the phase separator. (5) The forces that are produced by magnetic and mechanical unbalances must be minimized since gas bearings have a low tolerance to overloads. The use of multi-circuit parallel windings is a classical method of minimizing the unbalanced flux. In this particular case four circuits were used. Voltages are induced in the parallel armature windings and pole faces due to the existence of an unbalance in primary flux. These voltages produce circulating currents and a resultant flux field. This field, by Lenz's law, opposes and therefore minimizes the primary unbalanced flux.

Since the design of the rotor constituted a critical phase of the program, two tests were devised to verify the results of this effort. The first consisted of subjecting each rotor to a spin test of 51,000 rpm or 141 percent speed to produce 200 percent stress. After the spin test each rotor was checked for dimensional and balance changes in addition to reinspection of the braze joint. The second test consisted of driving the rotor at reduced speed in its stator. The saturation curves, when normalized to rated speed, compared favorably with the design calculations.

Table II summarizes the final design of the alternator. It is quite compact having a total weight of 51 pounds including the heat exchanger, end bells, and shaft extension. The rotor with a weight of approximately 12 pounds was kept small to minimize windage loss and problems in rotational dynamics. In general the design is conservative in that it is based on well established materials and fabrication techniques.

Figure 3 is a photograph of the completely assembled, alternator research package. Connectors for power leads, field current and thermocouples are evident at each end of the machine. The inlet and outlet ports for one coolant path can be seen on the side of the machine.

Figure 4 is a photograph of the alternator rotor. The magnetic and nonmagnetic sections of the rotor can be detected by the shading in the photograph. The slight taper of the pole side was introduced to minimize slot harmonics.

Figure 5 is a photograph of the major parts of the alternator. The end bell for the drive end is to the left, the rotor in the foreground and the stator with the anti-drive end bell in the background. The heat shield, to limit the flow of heat from the stator end turns to the rotor, can be seen clearly on the end bell for the drive end. The heavy bosses mounted on the stator are for accelerometers. The figure also shows that the overall rotor length is large when compared to the effective pole surface in the center.

Figure 6(a), (b), and (c) presents the characteristic and saturation curves for the alternator. These data were

measured with all field coils connected in series. Figure 6(a) shows the open circuit saturation, zero power factor saturation and three-phase short-circuit characteristic. The data indicates that the alternator can readily produce 120 amperes (300 percent current). Figure 6(b) and (c) compare the saturation characteristics at 0.75 and 1.0 power factor. As expected the effect of decreasing the power factor is to increase the required excitation. For both cases the generator readily produces 1.5 per-unit (150 percent) current, indicating that the magnetizing characteristics are entirely satisfactory.

The electromagnetic efficiency, which neglects windage and bearing friction, is shown in Fig. 7. The efficiency was determined by the separation of losses. Over the range from 0.25 to 1.0 per-unit load, the efficiency exceeds 87 percent for any power factor greater than 0.75. If the power range is limited to 0.40 to 1.05 per-unit, the efficiency exceeds 90 percent for any power factor greater than 0.75. The essentially constant core-loss is predominant at low power levels. The copper-losses, both armature and field, are predominant at higher power levels. The net result is very little change in efficiency over a large power range.

Figure 8(a) and (b) compares the armature hot spot and field coil temperatures as a function of load, for power factors of 0.75 and unity. It is evident as was expected, that deceased power factor reflects as increased temperature. The armature hot spot was in the stack at approximately one-half of the slot length. The data indicates that the machine is capable of delivering 1.25 per unit load at 0.75 power factor.

The magnetic performance, efficiency and thermal distribution indicate that the alternator is entirely suitable for application is a space power system.

CONTROLS

As stated earlier, all control devices in the electrical system utilize hardware characteristic of static systems. The rack-mounted breadboard voltage regulator and speed controller are shown in Fig. 9. The package to the right consists of one speed controller.

Figure 10 provides additional detail on the assembly of the breadboard units. The series-field controller is a self-contained unit located at the rear of the voltage regulator.

Series-Field Controller

The series-field controller, which basically consists of current transformers and a bridge rectifier, supplies excitation to the alternator for the purpose of maintaining system fault currents. The fault currents are maintained for a time sufficient for the protection logic to take positive corrective action. The minimum fault current capability deemed necessary in the system is three per unit with a duration of five seconds. The series-field control-

ler also reduces the load requirements on the voltage regulator by supplying a part of the alternator field ampere turns as needed by the system during normal loading. With rated (1PU) load on the alternator, approximately 50 percent of the total ampere-turns is supplied by this controller. During a three per-unit system fault, the series-field controller delivers 100 percent of the excitation requirements or approximately 375 watts. Output capacitors are provided in the controller to suppress voltage transients which may occur due to changes in system load.

Shunt-Field Regulator

The shunt-field regulator as shown in the block diagram, Fig. 11, operates in a switching mode. The regulator fundamentally consists of a voltage-sensor, a voltage-reference, a comparator, an amplifier, an output power stage, and a field-current limiter. The regulator senses the alternator output such that the average of the three-phase-voltages is held constant.

The DC output voltage of the sensor together with its superimposed line ripple is compared with a reference to drive the amplification and power stages at a frequency of 3600 pulses per second. This synchronization of the regulator function to the line occurs in the comparator by virtue of the line ripple. While operating within the active control range, the power-stage pulse width is proportional to the error voltage. This regulator synchronization to the line improves both the voltage-modulation level of the alternator output and the response time of the system when compared to the same regulator not synchronized to the line. The operating mode of the regulator dictates the need for a free-wheeling diode. The diode converts the pulse output of the regulator to a continuous shunt-field current. The regulator has a voltage gain of approximately 100. The current-limiter module limits the field current to an average of 5 amperes. Manual control of the the regulator can be obtained from an external source. This feature is provided in case an abnormal system operating mode should occur. The power losses in the shunt-field regulator when delivering rated output are shown in Table III.

Figure 12 is a plot of the voltage-regulator output (field current) against input line voltage. For this test, the sensing and power transformer inputs were connected together. The curve indicates that saturation of the output stage occurs at a very low input voltage, specifically 6.4 volts line to neutral. The increase in field current is linear with the increase in line voltage up to the setting of the field-current limiter. This limiting action is indicated at the right of the curve by the abrupt change in the current plot. For larger values of line voltage, the output current reduces, thus indicating the regulator is no longer saturated, but is switching on and off.

Speed-Controller

The speed-controller, as illustrated in block diagram

Fig. 13 consists of a transistorized frequency-sensor, a magnetic-amplifier and phase-controlled SCR power-output stages. The speed-controller effectively functions in a linear control mode in which the parasitic power is a function of line frequency.

The sensing stage which basically consists of two R-C networks including transistor switches develops a DC output current of sufficient magnitude to drive the first stage of magnetic amplification. The effect of the transistor switching is to modulate the energy level existing in each of the two networks. The sensor output current which is a function of transistor saturation time and therefore line frequency is proportional to the deviation of the frequency from a given set point.

Two stages of amplification are utilized in the speed-controller. Each stage consists of two full-wave magnetic-amplifiers in which the outputs are added differentially. The conduction angle of each amplifier with zero control is set to approximately 90 degrees by the use of leakage-reset control. This control mode tends to linearize the control characteristic and to reduce the effect of changes in ambient temperature. Gain adjustment is accomplished by controlling the feedback on the second stage.

The type of phase control (firing circuit) utilized in the output stage allows the gate-power dissipated in the SCR's to be minimized. The gate signal for all practical purposes goes to zero at the instant of SCR saturation. The controlling element in the firing circuit is a saturable reactor. The speed-controller has a power gain of approximately 800 watts per hertz.

Figure 14 is a plot for one speed-control unit of the power transfer characteristic against alternator speed (line frequency) as tested on the breadboard units. The curve illustrates the transfer characteristic in the active control range, the minimum shut-off losses, and the performance as a function of extreme changes in line frequency.

The power losses within the speed-controller are shown in Table III. The losses were measured at 1190 and 1220 hertz to make sure the controllers were fully-off and fully-on respectively.

The frequency-control range of each of the three controllers is shifted such that one controller is fully conducting prior to the turn-on of the succeeding controller. The power-frequency control curve, as shown in Fig. 15 illustrates the effect of this shift in control range. The amount of shift is indicated by the distance A.

The parasitic power capability of each controller when fully conducting is approximately 0.6 per unit or 1.8 per unit with three controllers.

Operation at this power level not only allows the generating system to continue functioning with one controller inoperative but also significantly reduces the recovery time of the system during system power transients. Multiple parasitic speed-controllers, as applied in this system, reduce the maximum volt-amp requirements on the alternator and the harmonic content of the alternator terminal voltage (2). Parasitic-type speed control is utilized to eliminate the need for control devices in the thermodynamic loop.

Manual control of the speed-controller can be obtained from an external source. This feature is provided in case an abnormal system operating mode should occur.

CONCLUSIONS

Experimental evaluation of a 1200-hertz alternator and its electrical controls designed for use in a Brayton-cycle space power system produced the following results:

1. Over a power range of 0.40 to 1.05 per unit, the alternator efficiency exceeds 90 percent for any power factor greater than 0.75.
2. The thermal characteristics are such that the alternator can deliver 1.25-per-unit power at 0.75 power factor.
3. The alternator readily produces 1.5-per-unit current at rated voltage, indicating that the magnetic characteristics are entirely satisfactory.
4. The shunt-field regulator delivers rated output current with an internal power dissipation of 41 watts.
5. The individual speed-controllers apply the maximum parasitic power (0.6 PU) with a 3-hertz change in line frequency.

REFERENCES

1. C. S. Corcoran and L. J. Yeager, "Development of Electric Components for a 400 Hertz Brayton Cycle Energy Conversion System," Advances in Energy Conversion Engineering, ASME, pp. 943-950, 1967.

2. L. J. Gilbert, "Reduction of Apparent-Power Requirement of Phase-Controlled Parasitically Loaded Turboalternator by Multiple Parasitic Loads," NASA TN D-4302, 1968.

TABLE I. – SYSTEM REQUIREMENTS

Voltage	120/208 3φ
Regulation	±1 percent
Response time ($\Delta E \leq \pm 5\% E_R$)	1/4 sec
Excursion (max)	136 percent*
Modulation	1/2 percent*
Drift (t ≥ 5 years)	1 volt
Harmonic content	5 percent*
Frequency	1200 hertz
Regulation	±1 percent
Response time ($\Delta F \leq \pm 2\% F_R$)	1 sec
Excursion (max)	±2 percent
Modulation	±2 hertz
Drift (t ≥ 5 years)	±2 hertz
Power range–optimum	2.25 to 10.5 kW
Overload rating	21 kVA for 5 sec
Short circuit rating	3 PU for 5 sec
Electrical Interference	MIL-STD-826
Design life (min)	5 years
Coolant temperatures	
Alternator	70° F (nom)
Controls	90° F (nom)
Environmental spec.	NASA P1224-1, -2
Neutron flux	≤ 10^{11} neutrons/cm^2
Integrated gamma dose	≤ 10^4 rads in 5 years

*Alternator – VR combination only.

TABLE III

Shunt-field regulator losses at rated I_{FLD}, 1200 hertz, 120 V_{L-N}	41 watts
Speed-controller losses (each unit)	
Minimum parasitic load at 1190 hertz, 120 V_{L-N}	13 watts
Maximum parasitic load at 1220 hertz, 120 V_{L-N}	300 watts

TABLE II. – FINAL DESIGN

A. Total weight (ARP)	51 pounds
Electromagnetic weight	35 pounds
B. Stator	
Circuits	4
Slots	36
Conductor	5 strands – No. 24 AWG
Conductors per slot	18
Turns per coil	9
Pitch factor	0.866
Distribution factor	0.96
Bore	3.3 inches
Stack length	1.65 inches
Slot pitch	0.288
Slot width	0.145
Tooth width	0.143
Current density at F. L.	6230 amps/inch^2
Flux density	
Teeth	87.9 kilolines/inch^2
Frame	84.6 kilolines/inch^2
C. Rotor	
Weight	11 pounds – 15 ounces
Outside diameter	3.26 inches
Pole length	1.65 inches
Diameter at auxiliary gap	2.150
Length at auxiliary gap	1.3
Pole embrace	0.667
Flux density – pole	86.5 kilolines/inch^2
D. Fields	
Outside diameter	5.584 inches
Inside diameter	4.284 inches
Length	1.7 inches
Conductor	No. 17 AWG
Current density at F. L.	1930 amps/inch^2
Shunt	
Turns	364
Resistance at 177° C	3.67 ohms
Current at 14.3 kVA	3.28 amperes
Series	
Turns	388
Resistance at 177° C	4.40 ohms
Current at 14.3 kVA	3.22 amperes
E. Main gap	0.020 inches
Main gap flux density	39.2 kilolines/inch^2
F. Auxiliary gap	0.020 inches
Auxiliary gap flux density	34.6 kilolines/inch^2
G. Materials	
Rotor poles	SAE 4340
Rotor interpole section	Inconel 718
Stator laminations	0.004 inch AL 4750
Frame	Annealed 1010 steel
Conductors	Copper
Conductor insulation	Polyimide enamel
Slot liner	0.010 Nomex
Separator	0.010 Nomex
Topstick	0.020 Nomex
Impregnant	Doryl
Non-magnetic separator	Copper
H. Coolant	DC-200

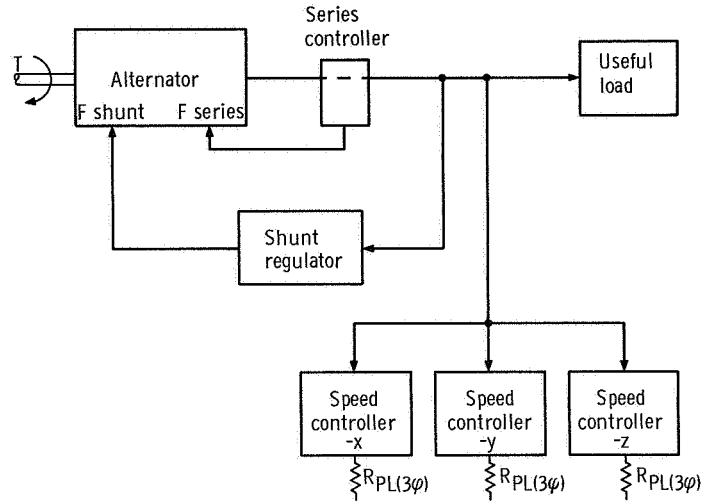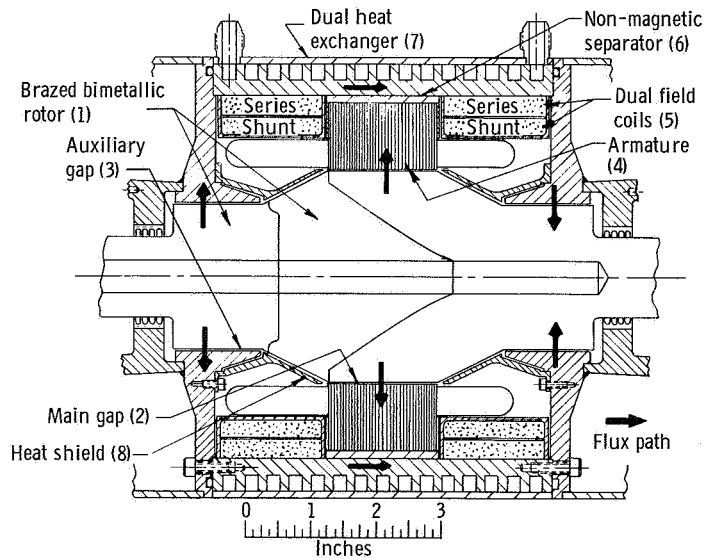Figure 1. - Block diagram of Brayton electrical system.

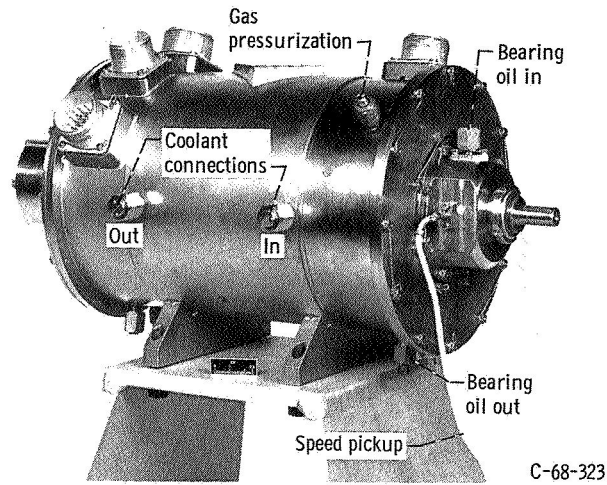Figure 2. - Sectional view of research alternator.

Gas
pressurization

Bearing
oil in

Coolant
connections

Out

In

Bearing
oil out

Speed pickup

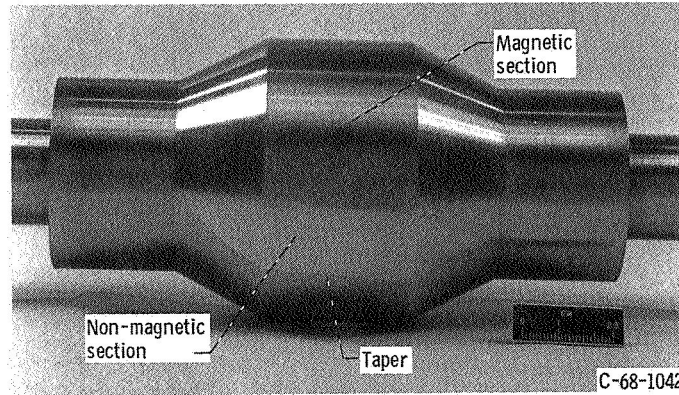C-68-323

Figure 3. - Research alternator.

Magnetic
section

Non-magnetic
section

Taper

C-68-1042

Figure 4. - Alternator rotor.

Accelerometer
bosses

Heat
shield

End
bell

Effective pole surface

C-68-466
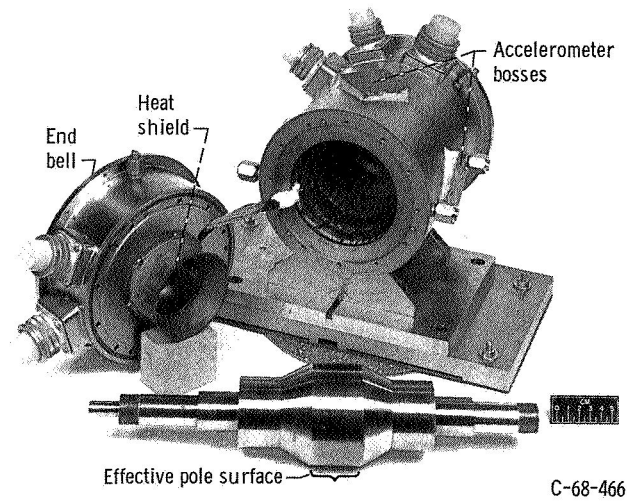
Figure 5. - Partially disassembled alternator.
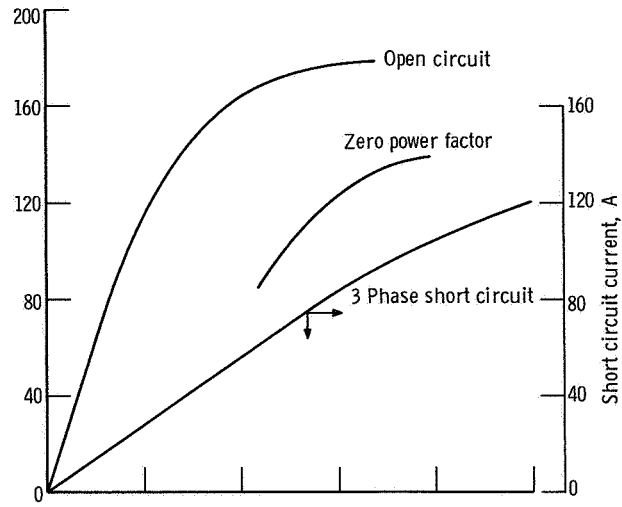
(a) Saturation curves.
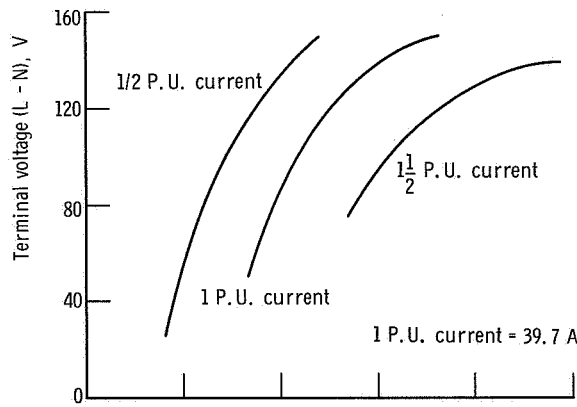
(b) Load saturation curves; 0.75 power factor.
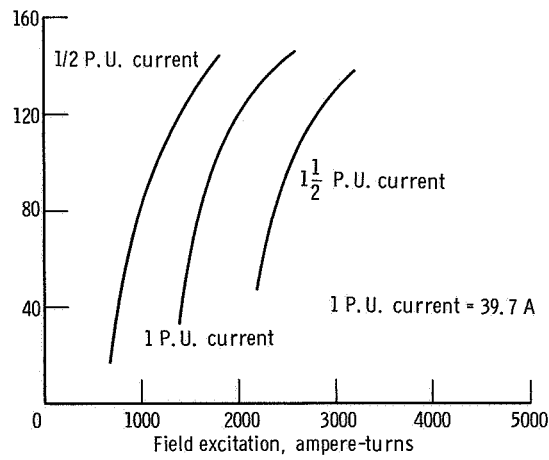
(c) Load saturation curves; unity power factor.

Figure 6. - 1200 Hertz Brayton cycle alternator magnetic characteristics.

Maximum allowable temperatures
for 5 year life
Armature - 220°
Field - 180°

Armature

1 per unit = 10.7 KW
Inlet oil temperature = 17° C

Field

(a) Armature and field temperatures for 0.75 power factor loads.

Armature

Field

(b) Armature and field temperature for unity power factor loads.

Alternator power output, per unit

Temperature, °C
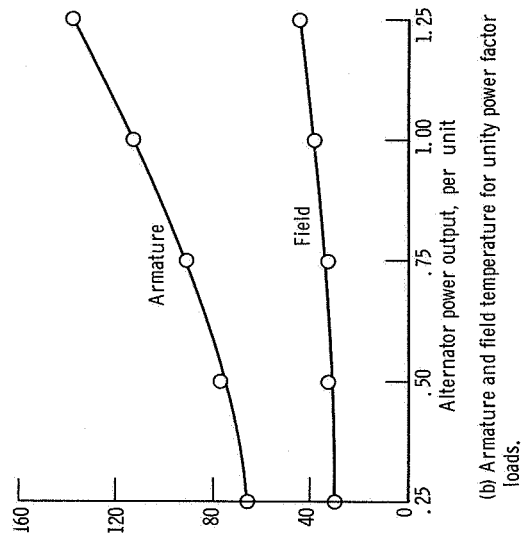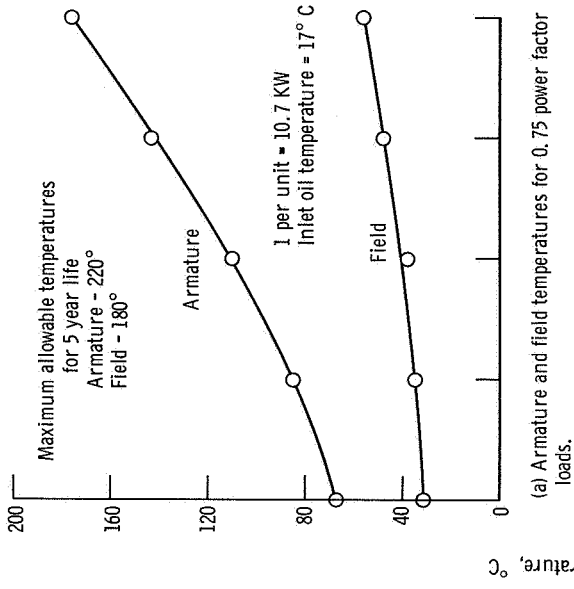
Figure 8. - 1200 Hertz Brayton cycle alternator.

1.0 P.F.

.75 P.F.

1 per unit = 10.7 kW
Inlet oil temperature = 17° C

Alternator power output, per unit

Efficiency, percent

Figure 7. - 1200 Hertz Brayton cycle alternator electro-magnetic efficiency.

Speed controller
(3 required)

Voltage regulator

C-68-461
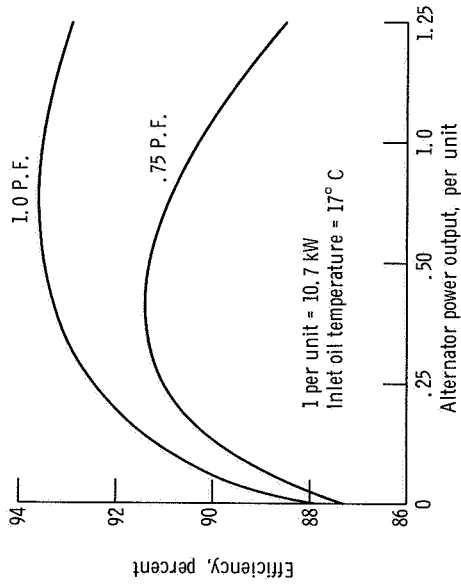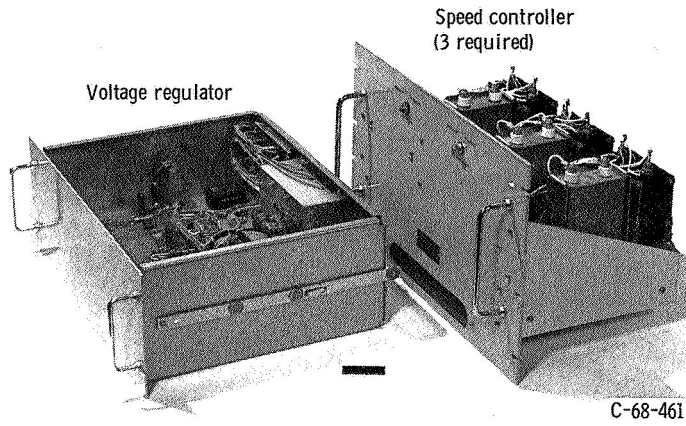
Figure 9. - Breadboard control devices.

Series field
controller

Voltage regulator

Speed controller

C-68-460
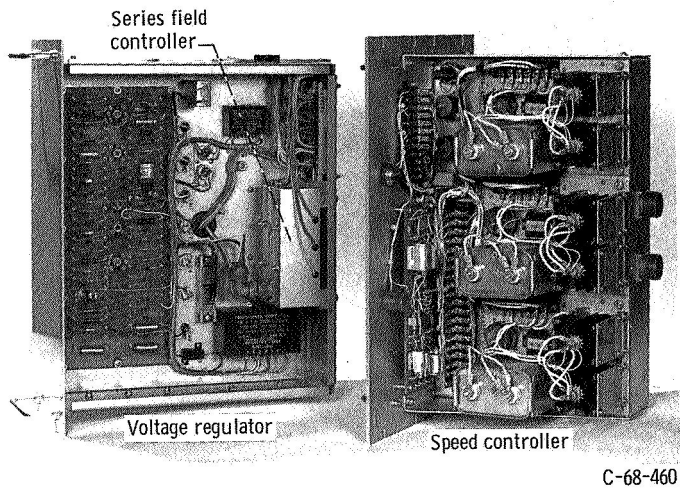
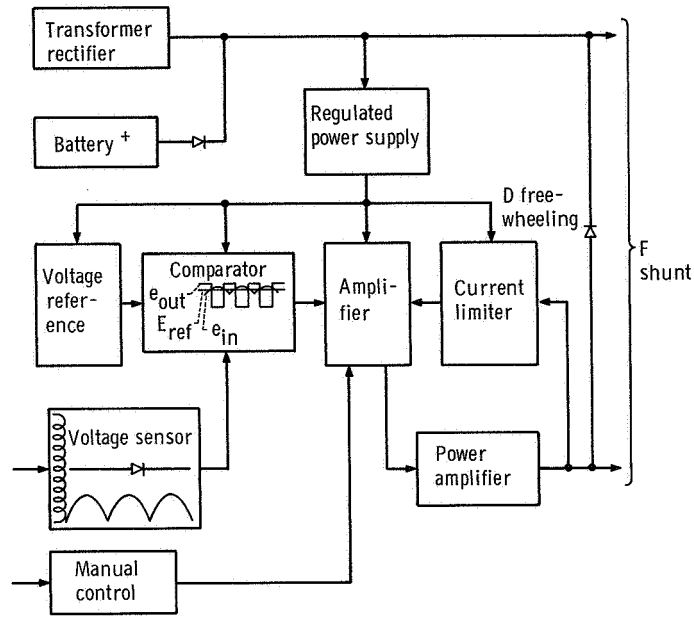Figure 10. - Detailed view of breadboard control devices.
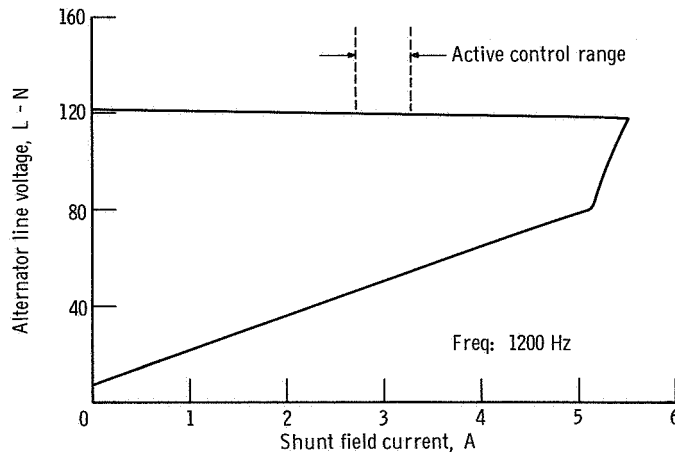
Figure 11. - Block diagram of shunt regulator.

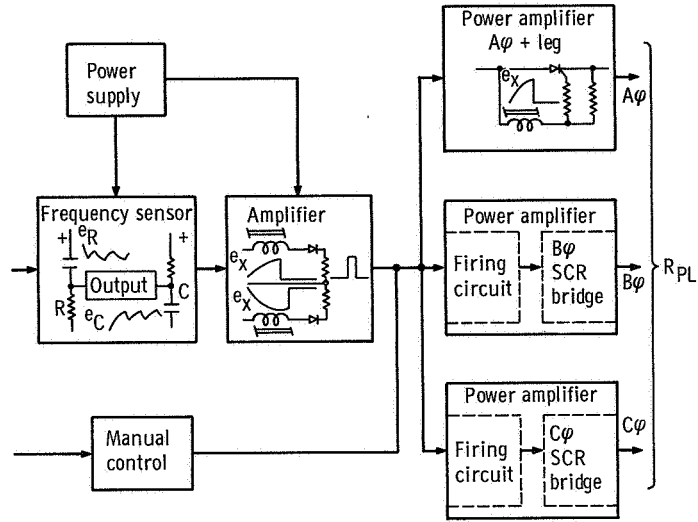Figure 12. - Shunt-field regulator characteristic.
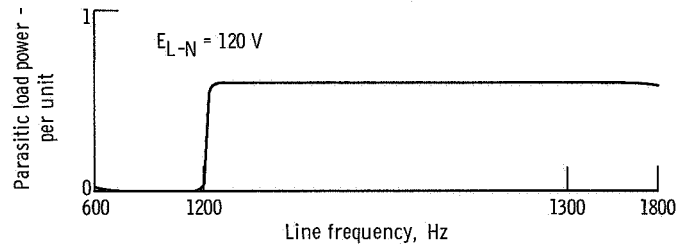
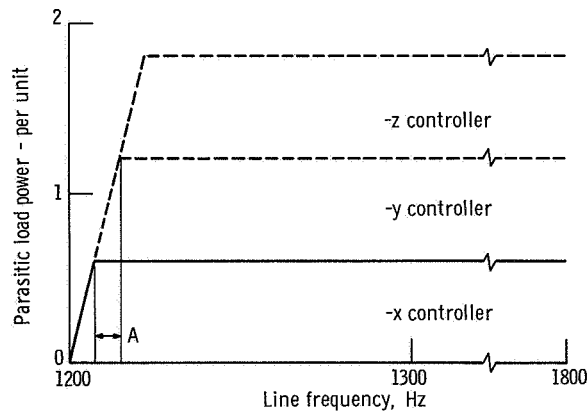Figure 13. – Block diagram of speed controller.

Figure 14. – Speed-controller characteristic.

Figure 15. – Speed-controller characteristic.